Engineering Science and Technology, an International Journal 19 (2016) 53–61

HOSTED BY

Contents lists available at ScienceDirect

Engineering Science and Technology, an International Journal

journal homepage: http://www.elsevier.com/locate/jestch

Full Length Article

Effect of chemical reaction on MHD boundary layer flow and melting heat transfer of Williamson nanofluid in porous medium

M.R. Krishnamurthy [a], B.C. Prasannakumara [b], B.J. Gireesha [a,c,*], Rama Subba Reddy Gorla [c]

[a] Department of Studies and Research in Mathematics, Kuvempu University, Shankaraghatta, Shimoga, Karnataka 577 451, India
[b] Government First Grade College, Koppa, Chikkamagaluru, Karnataka 577126, India
[c] Department of Mechanical Engineering, Cleveland State University, Cleveland, Ohio 44115, USA

ARTICLE INFO

Article history:
Received 18 May 2015
Received in revised form
24 June 2015
Accepted 29 June 2015
Available online 8 August 2015

Keywords:
Williamson nanofluid
Stretching surface
Melting heat transfer
Thermal radiation
Chemical reaction

ABSTRACT

Radiation and chemical reaction effects on the steady boundary layer flow of MHD Williamson fluid through porous medium toward a horizontal linearly stretching sheet in the presence of nanoparticles are investigated numerically. Adequate similarity transformations are used to derive a set of nonlinear ordinary differential equations governing the flow. The resultant nondimensionalized boundary value problem is solved numerically by Runge–Kutta–Fehlberg fourth–fifth order method with Shooting technique. The profiles for velocity, temperature and concentration, which are controlled by a number of thermophysical parameters, are presented graphically. Based on these plots the conclusions are given, and the obtained results are tested for their accuracy.

1. Introduction

Due to small size and very large specific surface areas of nanoparticles, nanofluids have superior properties like high thermal conductivity, minimal clogging in flow passages, long-term stability, and homogeneity. Thus, nanofluids have a wide range of potential applications in electronics cooling, pharmacological administration mechanisms, peristaltic pumps for diabetic treatments, solar collectors and nuclear applications. Initially, Choi and Eastman [1] presented the concept of nanofluids for suspension of liquids containing ultra-fine particles. Khan and Pop [2] in their first work on nanofluid have considered the problem on flow over stretching sheet. Gorla and Chamkha [3] have analyzed the problem on flow of nanofluid with natural convective boundary layer over a horizontal plate along with porous medium. Gireesha et al. [4,5] have studied the effects of dust particles suspended in a nanofluid flow past a stretching surface.

The non-Newtonian fluids are found in many engineering and industrial processes, such as food mixing and chyme movement in the intestine, flow of blood, flow of plasma, flow of mercury amalgams and lubrications with heavy oils and greases. Alam Khan and Khan [6] obtained the series solution by employing homotopy analysis method (HAM) in four flow problems of a Williamson fluid, namely Blasius, Sakiadis, stretching and stagnation point flows. Nadeem et al. [7,8] presented the modeling of a two-dimensional flow analysis for Williamson fluid over a linear and exponentially stretching surface. Hayat et al. [9] performed the series solution for the time independent MHD flow of Williamson fluid past a porous plate.

Non-Newtonian fluids are grouped property-wise, as visco-inelastic fluids, visco-elastic fluids, polar fluids, anisotropic fluids and fluids with micro-structure. Out of these Williamson fluid is one of visco-inelastic fluids. Although nanofluids have been largely studied as Newtonian fluid, very recently, their rheological properties are established by non-Newtonian modeling of nanofluid transport phenomena. Many studies are focused on non-Newtonian fluid as a base fluid with suspended nanoparticles over a stretching sheet. Rizwan et al. [10] have presented the nanoparticles analysis for the Casson fluid model by assuming the convective surface boundary conditions. Malik et al. [11] obtained the similarity solution for time independent boundary layer flow and heat transfer of a Casson nanofluid through an exponentially stretching cylinder. Jeffrey fluid has ability to exhibit the properties of ratio of stress relaxation to retardation. The steady flow of Jeffrey fluid model in

* Corresponding author. Tel.: +91 9741148002, fax: +91 08282256255.
E-mail address: g.bijjanaljayanna@csuohio.edu (B.J. Gireesha).
Peer review under responsibility of Karabuk University.

http://dx.doi.org/10.1016/j.jestch.2015.06.010

the presence of nano particles was studied by Nadeem et al. [12]. Shehzad et al. [13] developed a solar energy model to explore the characteristics of thermophoresis and Brownian motion in magnetohydrodynamic three-dimensional flow of nano Jeffrey fluid. In another investigation, Shehzad et al. [14] have observed the influence of nanoparticles in MHD flow of Jeffrey fluid over a stretched surface. They have considered the thermal and nanoparticles concentration convective boundary conditions. Hussain et al. [15] carried out an analysis to discuss heat and mass transfer analysis of two-dimensional hydromagnetic flow of an incompressible Jeffrey nanofluid over an exponentially stretching surface. Khan et al. [16] analyzed the free convective boundary-layer flow of three-dimensional Oldroyd-B nanofluid fluid over a bi-directional stretching sheet with heat generation/absorption. They have employed Oldroyd-B fluid model to describe the rheological behavior of viscoelastic nanofluid. Hayat et al. [17] obtained series solution using a well-known analytic approach, homotopy analysis method (HAM), for the flow of viscoelastic nanofluid over a stretching cylinder with simultaneous effects of heat and mass transfer. Nadeem and Hussain [18] have considered the two-dimensional flow of Williamson fluid over a stretching sheet and have discussed the effects of nano particles on Williamson fluid. Recently, Ramesh and Gireesha [19] studied the effects of heat source/sink on time independent boundary layer flow of a Maxwell fluid suspended with nanoparticles over a stretching sheet with convective boundary condition.

Over the last few years, a considerable amount of experimental and theoretical work has been carried out to determine the role of natural convection in the kinetics of heat transfer accompanied with melting or solidification effect. Processes involving melting heat transfer in non-Newtonian fluids have promising applications in thermal engineering, such as oil extraction, magma solidification, melting of permafrost, geothermal energy recovery, silicon wafer process, thermal insulation, etc. Roberts [20] was the first to describe the melting phenomena of ice placed in a hot stream of air at a steady state. Epstein and Cho [21] studied laminar film condensation on a vertical melting surface. Chamkha et al. [22] analyzed the effect of transverse magnetic field on hydromagnetic, forced convection flow with heat and mass transfer of a nanofluid over a horizontal stretching plate under the influence of melting and heat generation or absorption. Gorla et al. [23] presented a boundary layer analysis for a warm and laminar flow of nanofluid over a melting surface moving parallel to a uniform free stream. Prasannakumara et al. [24] studied melting phenomenon in MHD stagnation point flow of dusty fluid over a stretching sheet in the presence of thermal radiation and non-uniform heat source/sink.

Heat and mass transfer study on fluids with chemical reaction effect over a stretching sheet have important role in metallurgy and chemical engineering industries, such as food processing and polymer production. Moreover, coupled heat and mass transfer problems in the presence of chemical reaction are of importance in many processes, and have therefore received a considerable amount of attention in recent times. Possible applications can be found in processes such as drying, distribution of temperature and moisture over agricultural fields and groves of fruit trees, damage of crops due to freezing, evaporation at the surface of a water body and energy transfer in a wet cooling tower, and flow in a desert cooler.

Chamkha and Aly [25] obtained numerical solution of steady boundary-layer stagnation point flow of a polar fluid toward a stretching surface embedded in porous media in the presence of the effects of Soret and Dufour numbers and first-order homogeneous chemical reaction. Aurangzaib et al. [26] investigated the effect of thermal stratification and chemical reaction on free convection boundary layer MHD flow with heat and mass transfer of

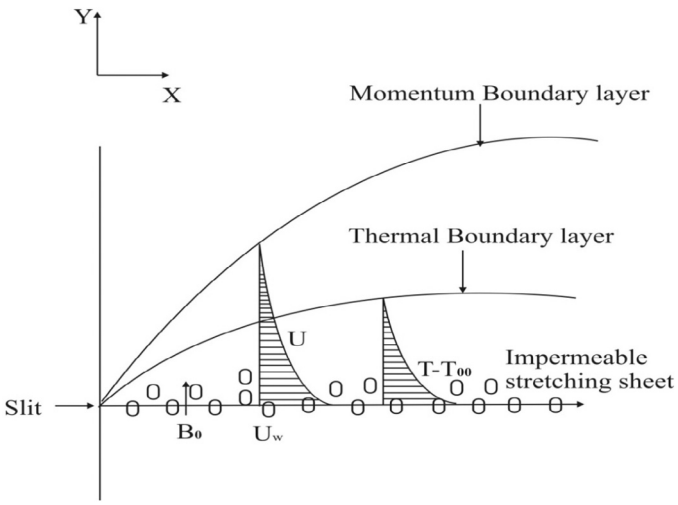

Fig. 1. Schematic diagram of boundary layer flow over stretching sheet.

an electrically conducting fluid over time dependent stretching sheet. Abd El-Aziz [27] obtained numerical results to study the effect of time-dependent chemical reaction on stagnation point flow and heat transfer of nanofluid over a stretching sheet. Pal and Mandal [28,29] investigated the mixed convection boundary layer flow of nanofluids at a stagnation-point over a permeable stretching/shrinking sheet subject to thermal radiation, heat source/sink, viscous dissipation and chemical reaction using numerical method.

Even though considerable progress has been made on flow phenomena over stretching sheet, more work is still needed to understand the effect of melting involving different non-Newtonian models and the formulation of accurate method of analysis for any body shape of engineering significance. The theoretical research on the topic, however, is hampered because of the complex nature of the equations describing the flows. The main emphasis of the present study is to discuss the nanoparticles analysis for the Williamson fluid model. Similarity transformation is used to reduce the governing equations of the problem into a system of nonlinear ordinary differential equations. The obtained similarity equations are then solved numerically using Runge–Kutta–Fehlberg–45 method with Shooting technique.

2. Mathematical formulation

Consider a two-dimensional steady flow of an incompressible Williamson nano fluid over a stretching surface embedded with porous medium. The plate is stretched along x-axis with a velocity ax, where $a>0$ is stretching parameter. The fluid velocity, temperature and nanoparticle concentration near surface are assumed to be U_w, T_w and C_w, respectively, which are as shown in Fig. 1. Further, let the temperature of the melting surface as T_m, and temperature in the free-stream condition as T_∞, where $T_\infty > T_m$. The viscous dissipation and the heat generation or absorption are assumed to be negligibly small.

For the present problem, the basic equations of conservation of mass, momentum, energy and concentration for a steady flow of nanofluid can be written in Cartesian coordinates x and y as,

$$\frac{\partial u}{\partial x}+\frac{\partial v}{\partial y}=0, \tag{2.1}$$

$$u\frac{\partial u}{\partial x}+v\frac{\partial u}{\partial y}=\nu\frac{\partial^2 u}{\partial y^2}+\sqrt{2}\nu\Gamma\frac{\partial u}{\partial y}\frac{\partial^2 u}{\partial y^2}-\frac{\sigma B^2{}_0}{\rho}u-\frac{\nu}{k'}u, \tag{2.2}$$

$$u\frac{\partial T}{\partial x}+v\frac{\partial T}{\partial y}=\alpha_m\frac{\partial^2 T}{\partial y^2}+\tau\left[D_B\frac{\partial C}{\partial y}\frac{\partial T}{\partial y}+\frac{D_T}{D_\infty}\left(\frac{\partial T}{\partial y}\right)^2\right]-\frac{1}{(\rho c)_f}\frac{\partial q_r}{\partial y}, \tag{2.3}$$

$$u\frac{\partial C}{\partial x}+v\frac{\partial C}{\partial y}=D_B\frac{\partial^2 C}{\partial y^2}+\frac{D_T}{D_\infty}\frac{\partial^2 T}{\partial y^2}-k_0C. \tag{2.4}$$

The corresponding boundary conditions are given by,

$$\begin{aligned}&u=U_w(x)=ax,\quad T=T_m,\quad C=C_w\quad\text{at}\quad y=0,\\&u=0\quad T\to T_\infty,\quad C\to C_\infty\quad\text{as}\quad y\to\infty,\quad\text{and}\\&k\left(\frac{\partial T}{\partial y}\right)_{y=0}=\rho[\beta+c_s(T_m-T_0)]v(x,0).\end{aligned} \tag{2.5}$$

Using Rosseland approximation for radiation, the radiative heat flux is simplified as,

$$q_r=-\frac{4\sigma^*}{3k^*}\frac{\partial T^4}{\partial y}, \tag{2.6}$$

where σ^* is Stefan–Boltzmann constant and k^* the mean absorption coefficient. The temperature differences within the flow are assumed to be small enough so that T^4 may be expressed as a linear function of temperature T using a truncated Taylor series about the free stream temperature T_∞, and neglecting the higher order terms we get,

$$T^4\approx 4TT^3{}_\infty-3T^3{}_\infty. \tag{2.7}$$

Substituting (2.6) and (2.7) in (2.3), we have

$$u\frac{\partial T}{\partial x}+v\frac{\partial T}{\partial y}=\alpha_m\frac{\partial^2 T}{\partial y^2}+\tau\left[D_B\frac{\partial C}{\partial y}\frac{\partial T}{\partial y}+\frac{D_T}{D_\infty}\left(\frac{\partial T}{\partial y}\right)^2\right]+\frac{16\sigma^*T^3{}_\infty}{3k^*(\rho c)_f}\frac{\partial^2 T}{\partial y^2}. \tag{2.8}$$

The governing equations can be reduced to ordinary differential equations, using the following similarity transformation,

$$\begin{aligned}&\psi=(a\nu)^{\frac{1}{2}}xf(\eta),\quad \eta=\left(\frac{a}{\nu}\right)^{1/2}y,\\&\theta(\eta)=\frac{T-T_m}{T_\infty-T_m},\quad \phi(\eta)=\frac{C-C_w}{C_\infty-C_w}.\end{aligned} \tag{2.9}$$

The stream function ψ is defined such that $u=\frac{\partial\psi}{\partial y}$ and $v=-\frac{\partial\psi}{\partial x}$.

With the help of above transformations, equation (2.1) is identically satisfied, and equations (2.2), (2.4) and (2.8) along with boundary conditions (2.5) take the following forms:

$$f'''+ff''-(f')^2+\lambda f'^2f'''-(Q+kp)f'=0, \tag{2.10}$$

$$\left(1+\frac{4}{3}R\right)\theta''\Big/Pr+f\theta'+Nb\phi'\theta'+Nt(\theta')^2=0, \tag{2.11}$$

$$\phi''+Lef\phi'+\frac{Nt}{Nb}\theta''-\gamma\phi=0, \tag{2.12}$$

where f, θ and ϕ are functions of η and prime denotes derivatives with respect to η. The corresponding boundary conditions will take the following form:

$$\begin{aligned}&f'(0)=1,\quad Prf(0)+M\theta'(0)=0,\quad \theta(0)=0,\quad \phi(0)=0,\\&f'(\infty)=0,\quad \theta(\infty)=1,\quad \phi(\infty)=1.\end{aligned} \tag{2.13}$$

The physical quantities of interest like skin friction coefficient (C_f), local Nusselt number (Nu_x) and local Sherwood number (Sh_x) are defined as

$$Nu_x=\frac{xq_w}{k(T_\infty-T_m)},\quad Sh_x=\frac{xq_m}{D_B(C_\infty-C_w)}\quad\text{and}\quad c_f=\frac{\tau_w}{\rho U_w^2}, \tag{2.14}$$

where the shear stress (τ_w), surface heat flux (q_w) and surface mass flux (q_m) are given by

$$q_w=-k\frac{\partial T}{\partial y},q_m=-D_B\frac{\partial C}{\partial y},\tau_w=\mu\left(\frac{\partial u}{\partial y}+\frac{\Gamma}{\sqrt{2}}\left(\frac{\partial u}{\partial y}\right)^2\right)\quad\text{at}\quad y=0. \tag{2.15}$$

Using the non-dimensional variables, we obtain

$$\begin{aligned}&Nu_x(Re_x)^{-\frac{1}{2}}=-\theta'(0),\quad C_f(Re_x)^{\frac{1}{2}}=f''(0)+\frac{\lambda}{2}f''(0)^2\quad\text{and}\\&Sh_x(Re_x)^{-\frac{1}{2}}=-\phi'(0)\end{aligned} \tag{2.16}$$

where $Re_x=\frac{xU_w(x)}{\nu}$ is the local Reynold's number.

3. Numerical procedure

The non-linear ordinary differential equations (2.10)–(2.12) with boundary conditions (2.13) have been solved using the Runge–Kutta–Fehlberg fourth–fifth order method with Shooting technique. A set of non-linear ordinary differential equations are of third order in f, second order in θ and ϕ, and are first reduced into a system of simultaneous ordinary equations. In order to solve this system using Runge–Kutta–Fehlberg fourth–fifth method, one should require three more missed initial conditions. However, the values of $f'(\eta),\theta(\eta),\phi(\eta)$ are known when $\eta\to\infty$. These end conditions are used to obtain unknown initial conditions at $\eta=0$ using Shooting technique. In shooting method, the boundary value problem is reduced to an initial value problem by assuming initial values. The boundary values calculated have to be matched with the real boundary values. Using trial and error or some scientific approach, one attempts to get as close to the boundary value as possible. The most essential step of this method is to choose the appropriate finite value for far field boundary condition. We took infinity condition at a large but finite value of η where no considerable variations in velocity, temperature and so on occur. We run our bulk computations with the value at $\eta_{max}=5$, which is sufficient to achieve the far field boundary conditions asymptotically for all values of the parameters considered.

To have a check on the accuracy of the numerical procedure used, first test computations for $\theta'(0)$ are carried out for viscous fluid for various values of Pr and compared with the available results of Khan and Pop [2], Golra and Sidawi [30], and Nadeem and Hussain [18] in Table 1, and they are found to be in excellent agreement.

Table 1
Comparison $\theta'(0)$ of viscous fluid for various values of Pr.

Pr	Khan and Pop [2]	Gorla and Sidawi [30]	Nadeem and Hussain [18]	Present
0.07	0.066	0.066	0.066	0.06624
0.20	0.169	0.169	0.169	0.16912
0.70	0.454	0.454	0.454	0.45432
2.0	0.911	0.911	0.911	0.91225

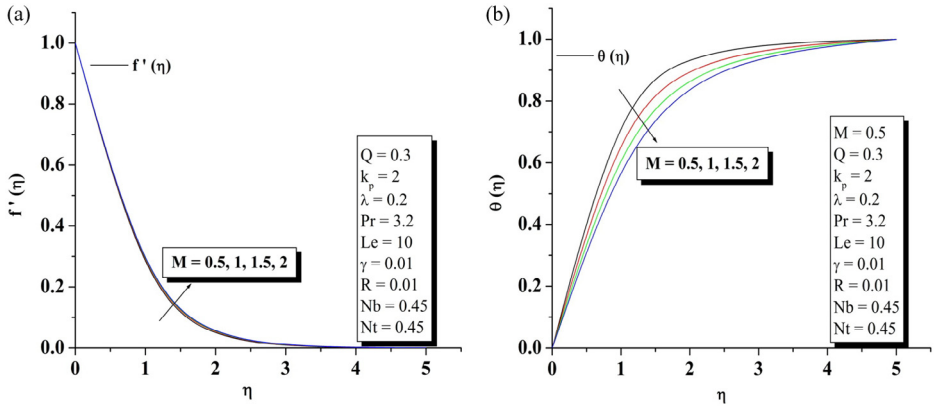

Fig. 2. (a) Effect of Melting parameter (M) on velocity profiles. (b) Effect of Melting parameter (M) on temperature profiles.

4. Results and discussion

The velocity, temperature and concentration profiles are obtained by solving equations (2.10)–(2.12) with boundary conditions (2.13) by assigning numerical values to the parameter encounter in the problem. Numerical values are expressed in terms of graphs to investigate the influence of various flow, controlling parameters like magnetic parameter, Prandtl number, radiation parameter, permeable parameter, chemical reaction parameter, melting parameter, Williamson parameter, Lewis number, Brownian motion and thermophoresis parameter.

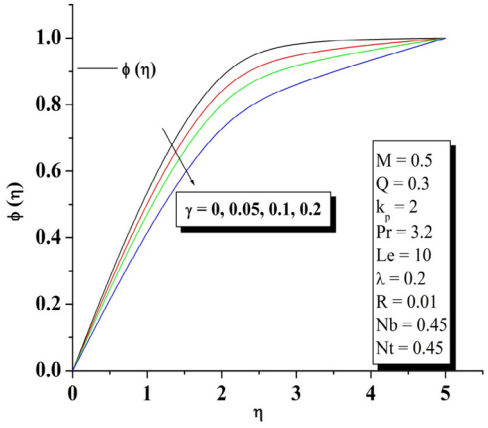

Fig. 3. Effect of Chemical reaction parameter (γ) on concentration profiles.

Fig. 2a and 2b reveals the velocity and temperature distributions for different values of melting parameter. It is observed that for increasing values of M, the velocity and the boundary layer thickness increase and decrease the temperature distribution. This is because an increase in M will increase the intensity of melting, which acts as blowing boundary condition at the stretching surface and hence tends to thicken the boundary layer. The variation of concentration profiles with chemical reaction parameter is shown in Fig. 3. It is observed that an increase in the value of chemical reaction parameter decreases the concentration of species in the boundary layer, whereas the velocity and temperature of the fluid are not significant with increase of chemical reaction parameter. This is due to the fact that chemical reaction in this system results in consumption of the chemical and hence results in decrease of concentration profile. The most important effect is that the first-order chemical reaction has a tendency to diminish the overshoot in the profiles of the solute concentration in the solutal boundary layer.

Fig. 4a and 4b explains the effect of radiation parameter on temperature and concentration profiles. It is observed that the temperature profile decreases and concentration profile increases for increasing values of R. This is because an increase in the radiation parameter R leads to decrease in the boundary layer thickness and enhances the heat transfer rate on melting surface in the presence of chemical effect. The effect of Lewis number (Le) on concentration and the temperature profiles are illustrated in Fig. 5a

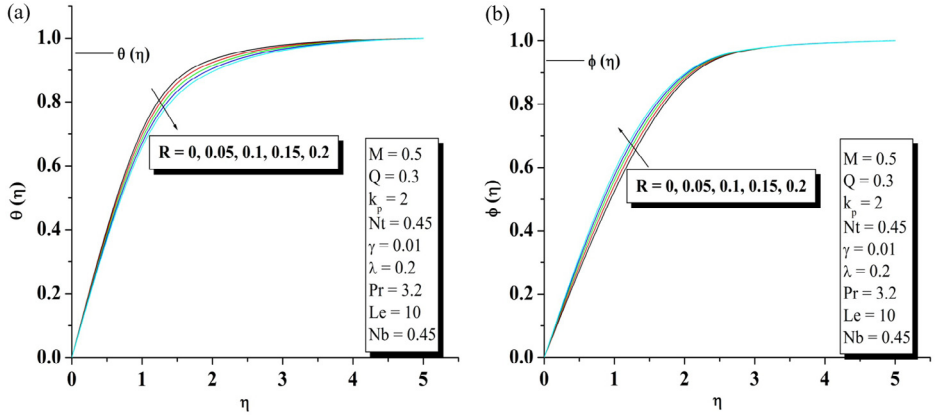

Fig. 4. (a) Effect of Radiation parameter (R) on temperature profiles. (b) Effect of Radiation parameter (R) on concentration profiles.

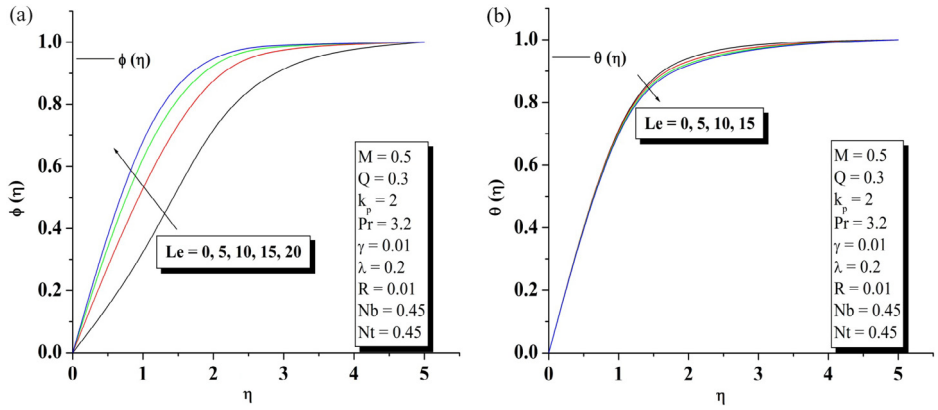

Fig. 5. (a) Effect of Lewis number (Le) on concentration profiles. (b) Effect of Lewis number (Le) on temperature profiles.

and 5b. It is clearly observed that the nanoparticles volume fraction as well as its boundary-layer thickness increase considerably as Le increases. We can also observe that temperature profiles decrease. Fig. 6 depicts the effect of Pr on temperature profiles. In the presence of melting parameter, an increase in Prandtl number increases the temperature profiles.

Fig. 7a and 7b depicts the effect of magnetic parameter (Q) on dimensionless velocity and temperature distributions, respectively. The presence of a magnetic field in an electrically conducting fluid induces a force called Lorentz force, which opposes the flow. This resistive force tends to slow down the flow, so the effect of increase in Q is to decrease the velocity and also causes increases in its temperature.

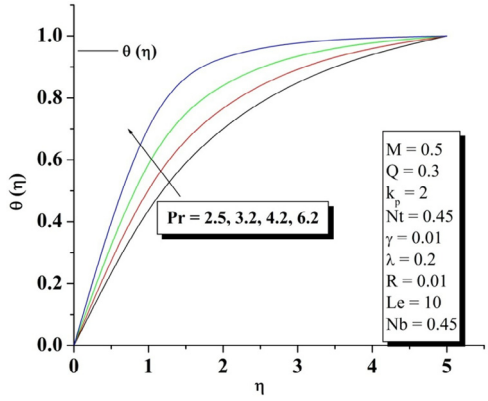

Fig. 6. Effect of Prandtl number (Pr) on temperature profiles.

The effects of Brownian motion (Nb) and thermophoresis parameter (Nt) on temperature and concentration profiles are depicted in Figs. 8a and 8b, and 9a and 9b, respectively. From these plots, it is observed that the effect of increasing values of (Nb) increases temperature profiles and decreases concentration profiles, whereas increasing values of (Nt) increases both the profiles. Fig. 10a and 10b demonstrates the effects of permeability parameter (k_p) on velocity profiles. It is obvious that the presence of porous medium causes higher restriction to the fluid flow, which in turn slows its motion. Therefore, with increasing permeability parameter, the resistance to the fluid motion increases and hence velocity decreases. Fig. 11a and 11b illustrates that the nanofluid velocity decreases with increase in non-Newtonian Williamson parameter (λ).

Fig. 12a and 12b is plotted to explain the effect of Williamson and melting parameter on skin friction coefficient and local Nusselt number. Here we have studied two cases, namely Williamson fluid in the presence and absence of nanoparticles. It can be seen that both $f''(0)+\frac{\lambda}{2}f''(0)^2$ and $\theta'(0)$ decreases with λ, whereas skin friction coefficient increases and local Nusselt number decreases with melting parameter, which is reasonable and expected from a physical point of view. It is interesting to note that, for both parameters, skin friction as well as local Nusselt number for Williamson fluid in the presence of nanoparticles are greater than that in the absence.

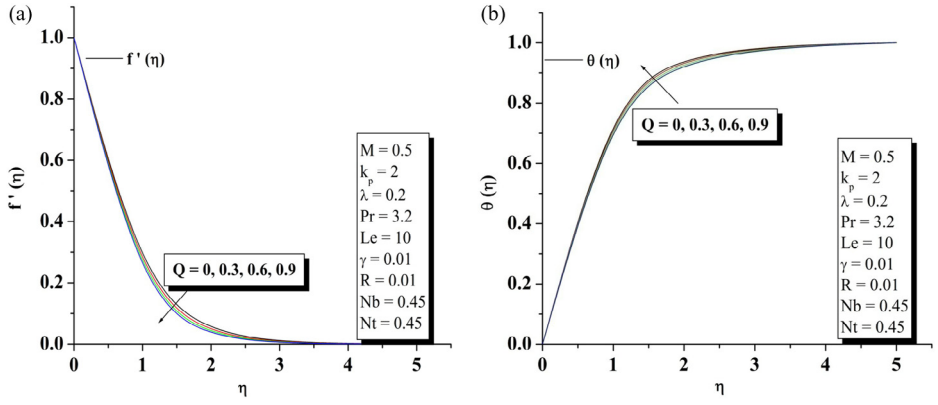

Fig. 7. (a) Effect of Magnetic parameter (Q) on velocity profiles. (b) Effect of Magnetic parameter (Q) on temperature profiles.

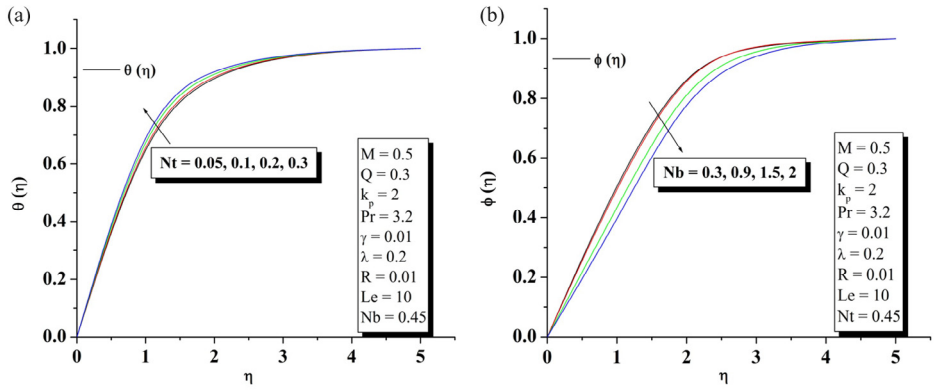

Fig. 8. (a) Effect of Brownian motion parameter (Nb) on temperature profiles. (b) Effect of Brownian motion parameter (Nb) on concentration profiles.

Fig. 13a and 13b is drawn to illustrate the influence of N_b, N_t on local Nusselt number and Sherwood number for both melting and non-melting surfaces. Both local Nusselt number and Sherwood number increases as N_b and N_t increases on melting and non-melting surfaces. The heat transfer shows very little change with N_b and N_t in the case of melting surfaces. Fig. 14 reveals that the heat transfer rate at the surface increases with Pr. This is due to the fact that a higher Prandtl number reduces the thermal boundary layer thickness and increases the surface heat transfer rate. Fig. 15a and 15b presents the effects of Lewis number (Le) and chemical reaction parameter (γ) on Nusselt number and Sherwood number with Pr and R. Both $\theta'(0)$ and $\phi'(0)$ increase with (Le) and decrease with (γ). Further, we can observe that $\theta'(0)$ decreases, whereas $\phi'(0)$ increases with radiation parameter R.

Variation of temperature gradient $[-\theta'(0)]$ and nanoparticle volume fraction gradient $[-\phi'(0)]$ with respect to permeability parameter (k_p), melting parameter (M, chemical reaction parameter (γ) and non Newtonian Williamson parameter (λ) are presented in Table 2. From this table, we can see that both $-\theta'(0)$ and $-\phi'(0)$ decrease with increasing values of k_p, M, γ and λ. Variation of skin friction coefficient with respect to non-Newtonian Williamson parameter (λ) and melting parameter (M) is given in Table 3. From this table, one can observe that the skin friction coefficient decreases with both (λ) and (M).

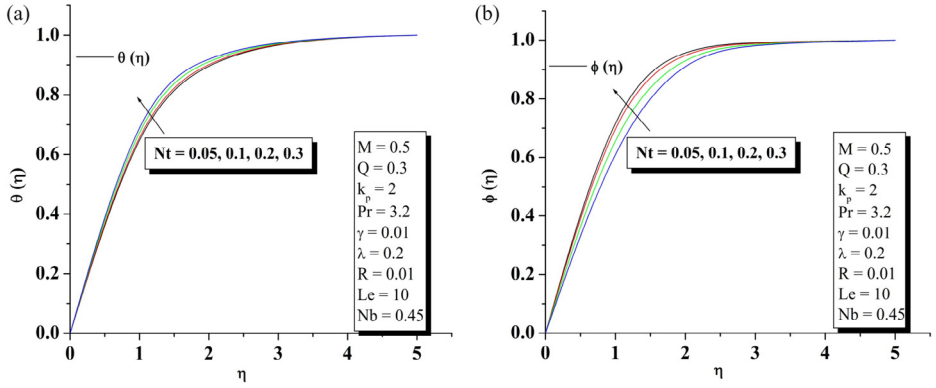

Fig. 9. (a) Effect of Thermophoresis parameter (Nt) on temperature profiles. (b) Effect of Thermophoresis parameter (Nt) on concentration profiles.

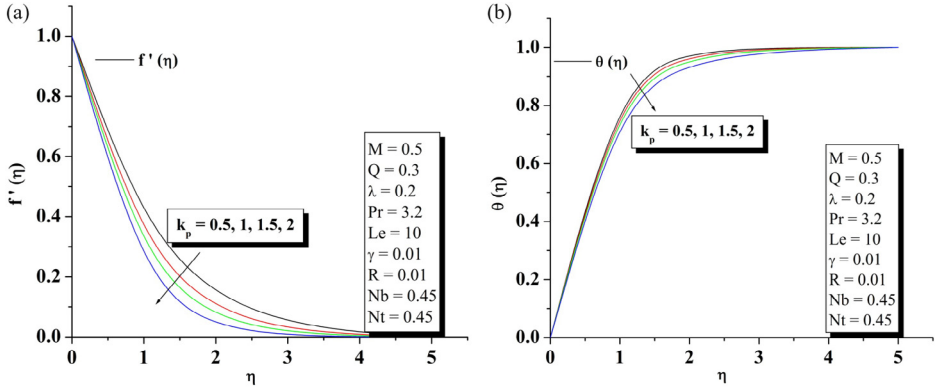

Fig. 10. (a) Effect of Permeability parameter (k_p) on velocity profiles. (b) Effect of Permeability parameter (k_p) on temperature profiles.

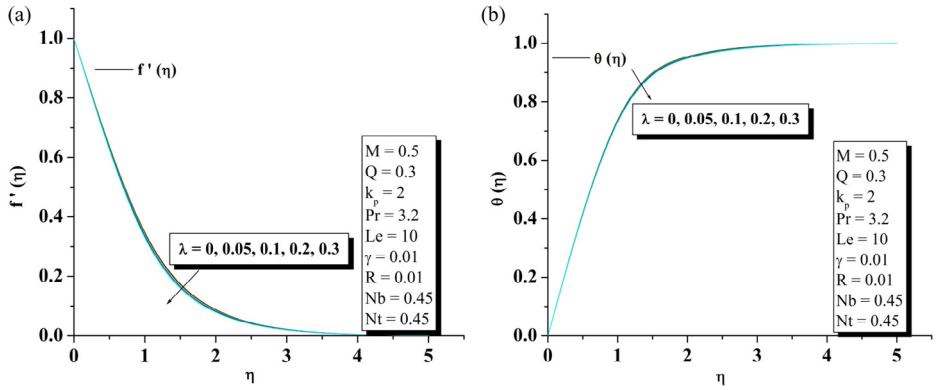

Fig. 11. (a) Effect of Williamson parameter (λ) on velocity profiles. (b) Effect of Williamson parameter (λ) on temperature profiles.

5. Conclusion

Melting, radiation and chemical reaction effects on a steady boundary layer flow of a Williamson fluid in the presence of nanoparticles toward a horizontal linearly stretching sheet are studied numerically. The transformed, non-linear ordinary differential equations governing the flow are solved numerically by Runge–Kutta–Fehlberg–45 method with Shooting technique. The results for velocity, temperature and concentration distributions are presented graphically for different values of the pertinent parameters. A chemical reaction is said to be first-order if the rate of reaction is directly proportional to concentration itself. The diffusive species can be generated or absorbed due to different types of chemical reaction with the ambient fluid, which can greatly affect the properties and quality of finished products. The influence of various parameters on the Nusselt number and skin friction coefficient is also examined. The most important results are summarized as follows:

- Velocity and the boundary layer thickness increase and temperature distribution decreases with increase in melting parameter.
- Chemical reaction parameter decreases the concentration profile, whereas the velocity and temperature of the fluid are not significant with increase of chemical reaction parameter.
- Temperature profile decreases and concentration profile increases for increasing values of radiation parameter.
- Magnetic parameter decreases the velocity and also causes increase in its temperature.

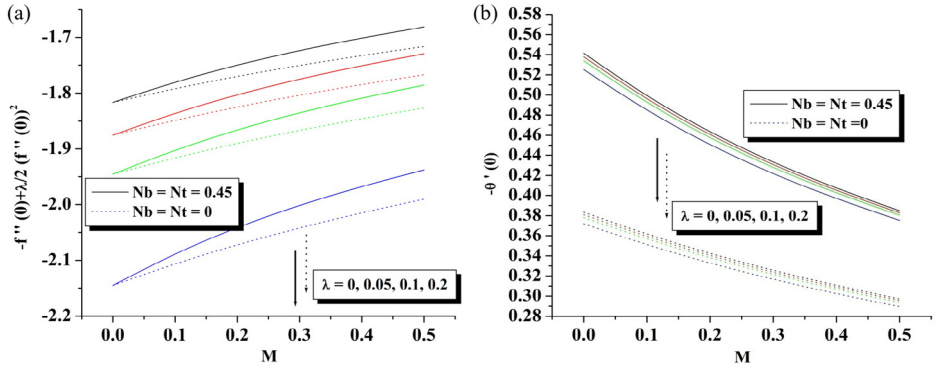

Fig. 12. (a) Effect of λ and M on skin friction coefficient. (b) Effect of λ and M on temperature gradient.

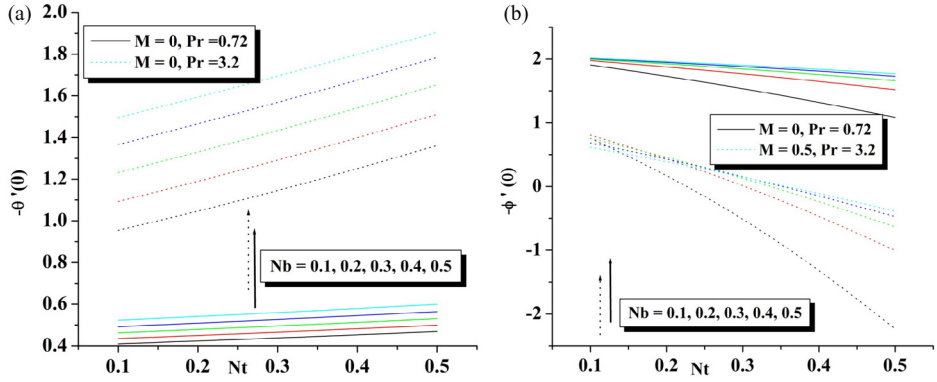

Fig. 13. (a) Effect of Nt and Nb on temperature ($-\theta'(0)$) gradients. (b) Effect of Nt and Nb on concentration ($-\phi'(0)$) gradients.

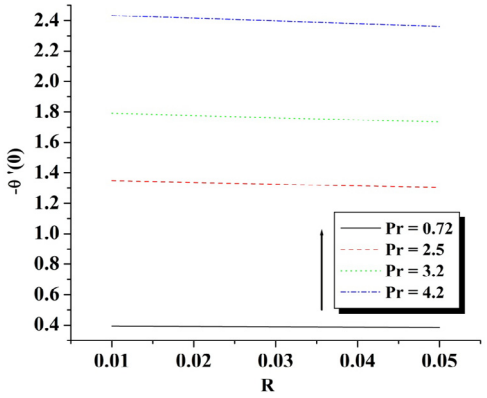

Fig. 14. Effect of Pr and R on temperature gradient ($-\theta'(0)$).

- Velocity profile decreases and temperature profile increases for increasing the values of permeability parameter.
- For increasing the values of Williamson parameter, velocity profile decreases and temperature profile increases.
- Temperature profile increases for increasing values of Nt and Nb.
- Temperature profile increases with the increasing values of Prandtl number.
- Skin friction coefficient as well as local Nusselt number for Williamson fluid in the presence of nanoparticles are greater than that in the absence.
- Local Nusselt number increases as N_b and N_t increase on melting and non-melting surfaces.
- The heat transfer shows very little change with N_b and N_t in case of melting surfaces.
- Both $\theta'(0)$ and $\phi'(0)$ increase with Lewis number, and as expected $\theta'(0)$ increases with Pr and $\phi'(0)$ decreases.

Acknowledgments

We would like to express our sincerest appreciation, indebtedness and thanks to the anonymous referees for their very expertise remarks and kind suggestions to improve the quality of manuscript. One of the authors (B.J. Gireesha) is thankful to the University Grants Commission, India, for the financial support (No. F 5-110/2014 (IC)) under the scheme of Raman Fellowship for Indian Scholars in USA. Further, B.C. Prasanna Kumara and M.R. Krishnamurthy are thankful to the University Grants Commission, India, for the financial support under the Major Research Project Scheme.

Table 2
Values wall temperature gradient ($-\theta'(0)$) and wall nano particle volume fraction gradient ($-\phi'(0)$) for different values of the parameters.

k_p	M	λ	γ	$-\phi'(0)$	$-\theta'(0)$
0	0.5	0.2	0.01	0.3345	2.1656
1				0.2975	1.9578
2				0.2698	1.7914
	0.5			0.2698	1.7914
	1			0.0920	1.1970
	2			0.0139	0.7392
		0.01		0.2780	1.8511
		0.1		0.2744	1.8256
		0.2		0.2698	1.7914
			0.05	0.2725	1.7661
			0.1	0.2761	1.7364
			0.2	0.2841	1.6832

Table 3
Values of $-\sqrt{Re}C_f$ for different values of λ and M.

λ	$M=0.3$	$M=0.6$	$M=1$	$M=1.5$	$M=2$
0.0	1.70978	1.66571	1.63308	1.60870	1.59262
0.05	1.68270	1.63955	1.60763	1.58379	1.56808
0.1	1.65384	1.61173	1.5806	1.55737	1.54206
0.15	1.62277	1.58185	1.55163	1.52910	1.51425
0.2	1.58884	1.54936	1.52022	1.49848	1.48416

Nomenclature

(u, v)	velocity components along the x and y axes
ρ	density of the nanofluid
$\alpha_m = \dfrac{k}{(\rho c)_f}$	nanofluid thermal diffusivity
ν	kinematic viscosity
D_B	Brownian diffusion coefficient
D_T	thermophoresis diffusion coefficient
T	nanofluid temperature
$(\rho c)_f$	heat capacity of the fluid
$(\rho c)_p$	effective heat capacity of the nanoparticle
B_0	induced magnetic field
k'	permeability of the porous medium
$\tau = \dfrac{(\rho c)_p}{(\rho c)_f}$	ratio between the effective heat capacity of the nanoparticle material and the fluid
k_0	chemical reaction coefficient
C	volumetric volume expansion coefficient
T_w	temperature of the nanofluid near wall
T_∞	free stream temperature of the nanofluid

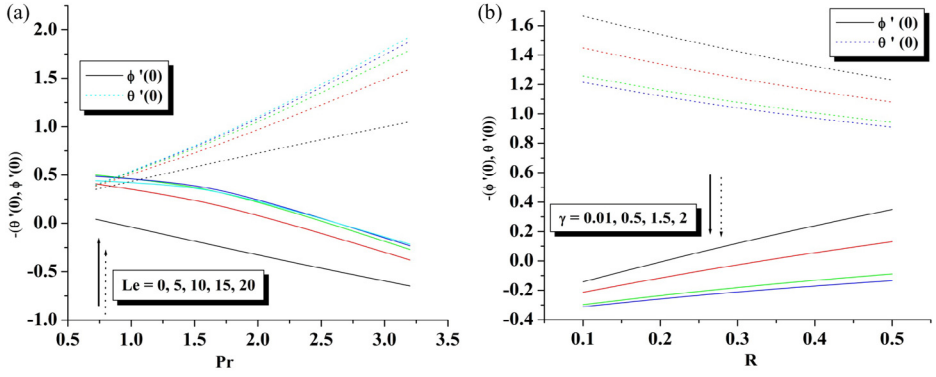

Fig. 15. (a) Effect of Le and Pr on temperature and concentration gradients. (b) Effect of γ and R on temperature and concentrations.

k	thermal conductivity
β	is the latent heat of the fluid
c_s	is the heat capacity of the solid surface
$U_w(x) = ax$	stretching sheet velocity
a	stretching rate being a positive constant
$\lambda = \Gamma x\left(\frac{2a^3}{\nu}\right)^{1/2}$	non-Newtonian Williamson parameter
$Q = \frac{\sigma B^2{}_0}{\rho a}$	magnetic parameter called Hartmann number
$k_p = \frac{\nu}{k'a}$	permeability parameter
$Pr = \frac{\nu}{\alpha_m}$	Prandtl number
$R = \frac{4\sigma^* T^3{}_\infty}{kk^*}$	Radiation parameter
$Nb = \frac{\tau D_B (C_\infty - C_w)}{\nu}$	Brownian motion parameter
$Nt = \frac{\tau D_T (T_\infty - T_m)}{\nu T_\infty}$	thermophoresis parameter
$Le = \frac{\nu}{D_B}$	Lewis number
$\gamma = \frac{k_0 U (C_\infty - C_w)}{\nu}$	chemical reaction parameter
$M = \frac{c_f (T_\infty - T_m)}{\beta + c_{s(T_m - T_0)}}$	dimensionless melting parameter
$\frac{c_f (T_\infty - T_m)}{\lambda}$ & $\frac{c_s (T_m - T_0)}{\lambda}$	Stefan number for the liquid and solid phases, respectively

References

[1] S.U.S. Choi, J.A. Eastman, Enhancing thermal conductivity of fluids with nanoparticles. The Proceedings of the ASME International Mechanical Engineering Congress and Exposition. ASME, San Francisco, USA, FED 231/MD 66, 99–105, 1995.

[2] W.A. Khan, I. Pop, Boundary-layer flow of a nanofluid past a stretching sheet, Int. J. Heat Mass Transf. 53 (2010) 2477–2483.

[3] R.S.R. Gorla, A. Chamkha, Natural convective boundary layer flow over a horizontal plate embedded in a porous medium saturated with a nanofluid, J. Mod. Phys. 2 (2011) 62–71.

[4] B.J. Gireesha, B. Mahanthesh, R.S.R. Gorla, Suspended particle effect on nanofluid boundary layer flow past a stretching surface, J. Nanofluids 3 (2014) 1–11.

[5] M.R. Krishnamurthy, B.C. Prasannakumara, B.J. Gireesha, R.S.R. Gorla, Effect of viscous dissipation on hydromagnetic fluid flow and heat transfer of nanofluid over an exponentially stretching sheet with fluid-particle suspension, Cogent Math. 2 (2015) 1050973.

[6] N. Alam Khan, H. Khan, A boundary layer flows of non-Newtonian Williamson fluid, Nonlinear Eng. 3 (2) (2014) 107–115.

[7] S. Nadeem, S.T. Hussain, C. Lee, Flow of a Williamson fluid over a stretching sheet, Braz. J. Chem. Eng. 30 (3) (2013) 619–625.

[8] S. Nadeem, S.T. Hussain, Heat transfer analysis of Williamson fluid over exponentially stretching surface, Appl. Math. Mech. Engl. Ed. 35 (4) (2014) 489–502.

[9] T. Hayat, U. Khalid, M. Qasim, Steady flow of a Williamson fluid past a porous plate, Asia Pac. J. Chem. Eng. 7 (2012) 302–306.

[10] U.H. Rizwan, S. Nadeem, Z.H. Khan, T.G. Okedayo, Convective heat transfer and MHD effects on Casson nanofluid flow over a shrinking sheet, Cent. Eur. J. Phys. 12 (12) (2014) 862–871.

[11] M.Y. Malik, M. Naseer, S. Nadeem, A. Rehman, The boundary layer flow of Casson nanofluid over a vertical exponentially stretching cylinder, Appl. Nanosci. 4 (2014) 869–873.

[12] S. Nadeem, R.U. Haq, Z.H. Khan, Numerical solution of non-Newtonian nanofluid flow over a stretching sheet, Appl. Nanosci. 4 (2014) 625–631.

[13] S.A. Shehzad, T. Hayat, A. Alsaedi, M.A. Obid, Nonlinear thermal radiation in three-dimensional flow of Jeffrey nanofluid: a model for solar energy, Appl. Math. Comput. 248 (2014) 273–286.

[14] S.A. Shehzad, T. Hayat, A. Alsaedi, MHD flow of Jeffrey nanofluid with convective boundary conditions, J. Braz. Soc. Mech. Sci. Eng. 37 (2015) 873–883, doi:10.1007/s40430-014-0222-3.

[15] T. Hussain, S.A. Shehzad, T. Hayat, A. Alsaedi, F. Al-Solamy, Radiative hydromagnetic flow of Jeffrey nanofluid by an exponentially stretching sheet, PLoS ONE 9 (8) (2014) e103719, doi:10.1371/journal.pone.0103719.

[16] W.A. Khan, M. Khan, R. Malik, Three-dimensional flow of an Oldroyd-B nanofluid towards stretching surface with heat generation/absorption, PLoS ONE 9 (8) (2014) e105107, doi:10.1371/journal.pone.0105107.

[17] T. Hayat, M. Bilal Ashraf, S.A. Shehzad, N.N. Bayomi, Mixed convection flow of viscoelastic nanofluid over a stretching cylinder, J. Braz. Soc. Mech. Sci. Eng. 37 (2015) 849–859, doi:10.1007/s40430-014-0219-y.

[18] S. Nadeem, S.T. Hussain, Flow and heat transfer analysis of Williamson nanofluid, Appl. Nanosci. 4 (2014) 1005–1012, doi:10.1007/s13204-013-0282-1.

[19] G.K. Ramesh, B.J. Gireesha, Influence of heat source/sink on a Maxwell fluid over a stretching surface with convective boundary condition in the presence of nanoparticles, Ain Shams Eng. J. 5 (2014) 991–998.

[20] L. Roberts, On the melting of a semi-infinite body of ice placed in a hot stream of air, J. Fluid Mech. 4 (1958) 505–528.

[21] M. Epstein, D.H. Cho, Melting heat transfer in steady laminar flow over a flat plate, J. Heat Transf. 98 (3) (1976) 531–533.

[22] A.J. Chamkha, A.M. Rashad, E. Al-Meshaiei, Melting effect on unsteady hydromagnetic flow of a nanofluid past a stretching sheet, Int. J. Chem. React. Eng. 9 (2011) 1–13.

[23] R.S.R. Gorla, A. Chamkha, A. Aloraier, Melting heat transfer in a nanofluid flow past a permeable continuous moving surface, J. Nav. Arch. Mar. Eng. 2 (2011) 83–92.

[24] B.C. Prasannakumara, B.J. Gireesha, P.T. Manjunatha, Melting phenomenon in MHD stagnation point flow of dusty fluid over a stretching sheet in the presence of thermal radiation and non-uniform heat source/sink, Int. J. Comput. Methods Eng. Sci. Mech. (2015) doi:10.1080/15502287.2015.1047056. In press.

[25] A.J. Chamkha, A.M. Aly, Heat and mass transfer in stagnation point flow of a polar fluid towards a stretching surface in porous media in the presence of Soret, Dufour and chemical reaction effects, Chem. Eng. Commun. 198 (2) (2010) 214–234.

[26] Aurangzaib, A.R.M. Kasim, N.F. Mohammad, S. Shafie, Effect of thermal stratification on MHD free convection with heat and mass transfer over an unsteady stretching surface with heat source, Hall current and chemical reaction, Int. J. Adv. Eng. Sci. Appl. Math. 4 (3) (2012) 217–225.

[27] M. Abd El-Aziz, Effect of time-dependent chemical reaction on stagnation point flow and heat transfer over a stretching sheet in a nanofluid, Phys. Sci. 89 (2014) 085205.

[28] D. Pal, G. Mandal, Influence of thermal radiation on mixed convection heat and mass transfer stagnation-point flow in nanofluids over stretching/shrinking sheet in a porous medium with chemical reaction, Nuclear Eng. Design 273 (2014) 644–652.

[29] D. Pal, H. Mondal, MHD non-Darcian mixed convection heat and mass transfer over a non-linear stretching sheet with Soret–Dufour effects and chemical reaction, Int. Commun. Heat Mass Transf. 38 (2011) 463–467.

[30] R.S.R. Gorla, I. Sidawi, Free convection on a vertical stretching surface with suction and blowing, Appl. Sci. Res. 52 (1994) 247–257.